Final Report

IR DETECTORS TECHNOLOGY

Project:

SPC-99-4060

July 2000

Issuing Organization and Point of Contact

Institute of Physics, Charles University

Prof.Pavel Höschl

Ke Karlovu 5
CZ-121 16 Prague 2
Czech Republic
FAX (+420 2) 296764

REPORT DOCUMENTATION PAGE

Form Approved OMB No. 0704-0188

1. AGENCY USE ONLY (Leave blank)	2. REPORT DATE	3. REPORT TYPE AND DATES COVERED
	July 2000	Final Report

4. TITLE AND SUBTITLE

IR Detectors Technology

5. FUNDING NUMBERS

F61775-99-WE060

6. AUTHOR(S)

Professor Pavel Hoschl

7. PERFORMING ORGANIZATION NAME(S) AND ADDRESS(ES)

Charles University
Institute of Physics
PRAGUE 2 CZ-121 16
Czech Republic

8. PERFORMING ORGANIZATION REPORT NUMBER

N/A

9. SPONSORING/MONITORING AGENCY NAME(S) AND ADDRESS(ES)

EOARD
PSC 802 BOX 14
FPO 09499-0200

10. SPONSORING/MONITORING AGENCY REPORT NUMBER

SPC 99-4060

11. SUPPLEMENTARY NOTES

12a. DISTRIBUTION/AVAILABILITY STATEMENT

Approved for public release; distribution is unlimited.

12b. DISTRIBUTION CODE

A

13. ABSTRACT (Maximum 200 words)

This report results from a contract tasking Charles University as follows: The contractor will prepare Near perfect (CdZn)Te crystals of diameter up to 10 cm under a defined Cd overpressure. Modeling of the crystal growth process will be performed to optimize conditions for the growth of perfect crystals. The objective is to produce near-perfect (CdZn)Te substrates in orientations (111) and (211) for LPE/MBE epitaxial growth applications. Point defects will be studied by galvanomagnetic and optical measurements. The aim of the experiments is to find out, how the composition of the melt close to the melting point and the way of cooling down the crystal after solidification influences its optical and electrical properties and concentration of precipitates.

14. SUBJECT TERMS

EOARD, Sensor Technology, Detector Technology

15. NUMBER OF PAGES

43

16. PRICE CODE

N/A

17. SECURITY CLASSIFICATION OF REPORT	18. SECURITY CLASSIFICATION OF THIS PAGE	19. SECURITY CLASSIFICATION OF ABSTRACT	20. LIMITATION OF ABSTRACT
UNCLASSIFIED	UNCLASSIFIED	UNCLASSIFIED	UL

Distribution:	Dr. William Frederick	1 copy
	Jay Howland, M.Sc.	1 copy

Content

I. INTRODUCTION

This final report contains the results of the project SPC-99-4060 and concentrates mainly on a summary of high temperature defect structure of CdTe and defect modeling. Some results already presented in the Progress Report submitted in January 2000 were extended and an improved evaluation and discussion of experimental data was performed. High temperature defect equilibrium was studied on both the Cd and Te sides of the P-T diagram and a complex theoretical approach is presented. The main effort concentrated on in-situ galvanomagnetic measurements in the liquid CdTe, where in the case of measurements of Hall effect no experimental data were published so far. The results of crystal growth, characterization of crystals grown under different conditions by optical methods and modeling of crystal growth were given in the Progress report.

The wide-bandgap binary semiconductor CdTe (CT) with the bandgap 1.5 eV at room temperature is used as a source material for preparation of detectors of gamma radiation, as a substrate for fabrication of detectors of infrared radiation on the basis of (CdHg)Te and also as a material for electrooptical modulation of signals. The recent progress in high technology brings a renewed interest to the research of basic properties of CT [1,2].

In order to optimize the function of the devices it is necessary to improve both structural and material parameters of the single crystalline CT. According to the state-of-the-art of technology of growth of CT single crystals, both demands lead to minimization of influence of native point defects, which can affect e.g. the room temperature mobility and lifetime of carriers or the concentration of precipitates of one of the components (Cd,Te) at higher defect concentrations. To prepare the high quality single crystalline CT it is necessary to know the equilibrium concentrations of point defects and diffusion processes, which establish the equilibrium concentrations during cooling/heating or when the pressure of one of the components above the crystal is changed. The real-time-diffusion occurs at temperatures above 500°C.

The equilibrium concentration of electrically active point defects in the whole region of

stability of the solid phase depends on the temperature and pressure of one of the components. It implies, that the concentration of free carriers in the sample changes in the dependence on both the temperature and the pressure of one of the components, e.g. Cd, as well. The equilibrium concentrations of defects can be experimentally studied *in-situ* at high temperature by the measurement of the Hall coefficient R_H and conductivity σ, from which the Hall mobility $\mu_H = R_H\sigma$ is calculated.

The measurement of R_H and σ can be performed by two ways. In the first way the sublimation of the more volatile component (Cd) is prevented by the sample encapsulation, e.g. by Si_3N_4 deposited in a pyrolytic reactor. The content of Cd and Te does not change and only the temperature dependence is studied in this case. In the second method, which is used in our case, the content of Cd in the sample changes due to the sublimation from the free surface. The equilibrium is controlled here by a proper Cd overpressure which is established in the two-zone furnace by a temperature of the Cd source. The advantage of this arrangement is the possibility to measure properties of CT in the phase P-T diagram both in intrinsic conditions and under Cd or Te overpressure. The measurement of R_H and σ is performed in dependence on the pressure and temperature of Cd when the equilibrium concentration of electrically active defects is established by diffusion processes. Experimental data show as expected, that R_H and σ depend both on pressure of Cd and temperature, but the μ_H is near intrinsic conditions practically independent of Cd pressure P_{Cd}. It implies that there is not important impurity scattering in this case. Figure 1 shows the phase P-T diagram for CT with a marked region of stability of CT, where our measurements were performed (Cd-rich area of the phase diagram).

II. EXPERIMENT

The measurement was performed on samples from single crystals prepared by vertical cooling in the temperature gradient. The high temperature measurements were done in a quartz ampoule with a diameter 17 mm located in a furnace

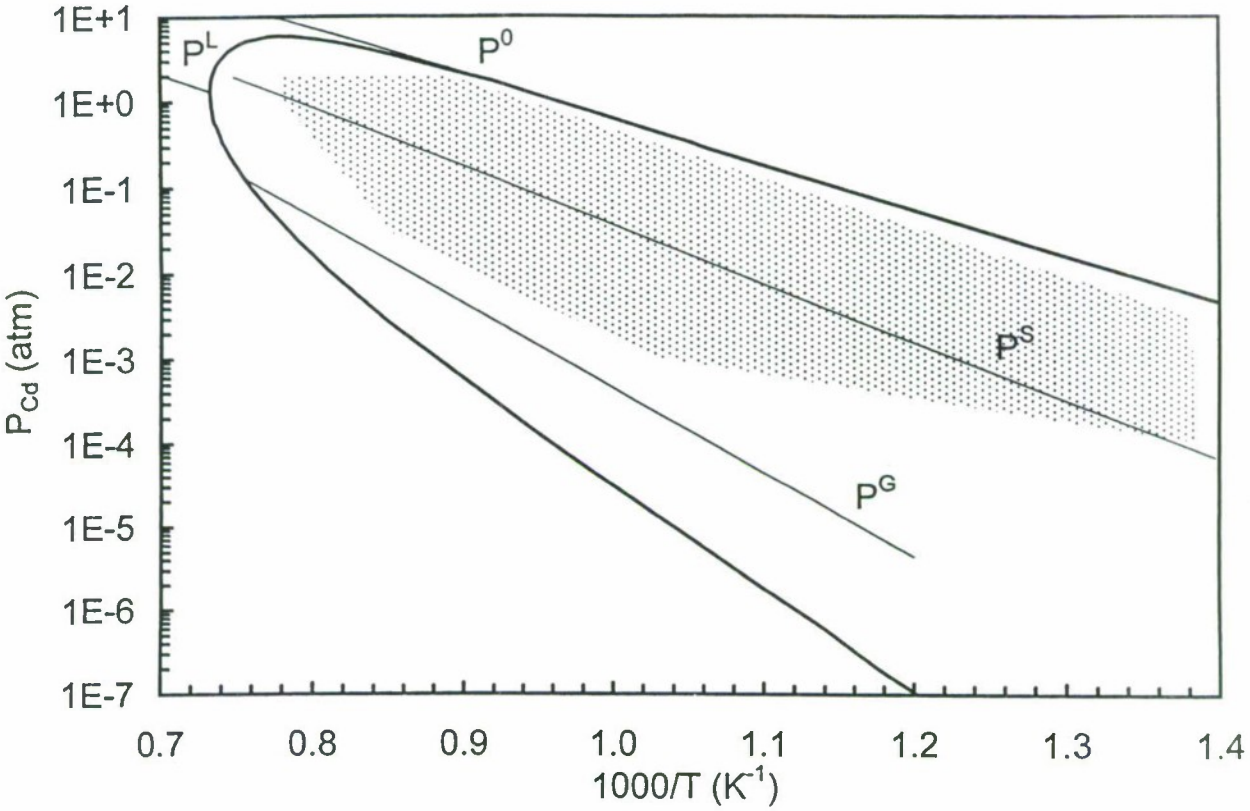

Fig.1. The P-T phase diagram of CdTe with the marked area (dotted) at which the measurements were performed. P^S, P^G, and P^L plot the solidus, gasus, and liquidus stoichiometry condition, respectively. P^0 is the Cd partial pressure over pure Cd.

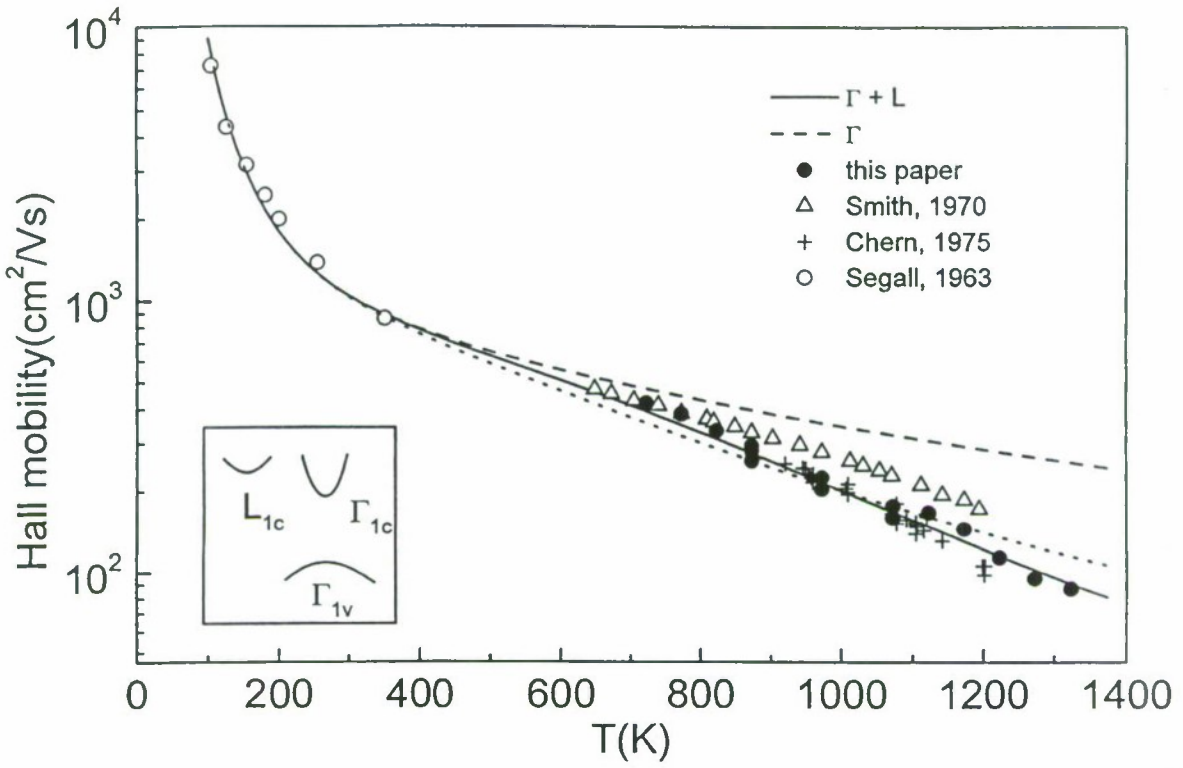

Fig.2. Experimental and theoretical data of Hall mobilities in CdTe. The low temperature points (o) are according to Ref. [3]. Our high temperature experiment (•) is shown together with previous measurements (△) [6] and (+) [7]. Our data confirm the measurements of [7]. The full line draws the best theoretical fit. The dash line is without effect of the L-valley. The dotted line is for temperature independent $\Delta E = 0.19$ eV. The inset plots the scheme of the model band structure.

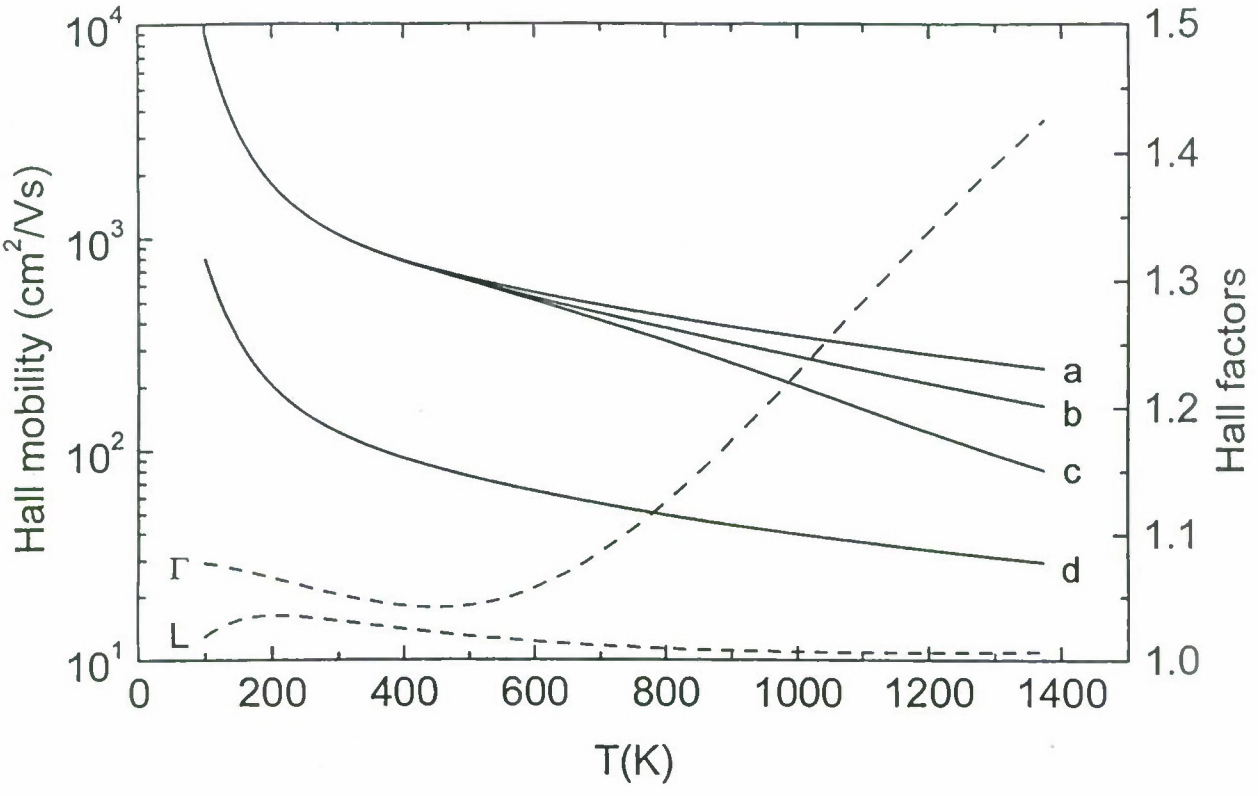

Fig.3. The Hall mobilities within different types of scattering included (left axis, full) and the conduction band Hall factors (right axis, dash). The mobility μ_Γ without effect of the L-valley - (line a). The mobility μ_Γ including the intervalley scattering - (line b). The total Hall electron mobility - (line c). The mobility μ_L - (line d). r_Γ - (line Γ), r_L - (line L).

It was possible to keep the sample temperature with the precision of about 1°C and to change the gas pressure of one of the components (in our case Cd) in the interval 2×10^{-4} – 2 atm. The sample with tungsten or molybdenum spring contacts in the van der Pauw configuration was placed in a quartz holder together with the Pt-PtRh thermocouple.

III. HIGH TEMPERATURE MOBILITY

A. Model and Theory

We shall concentrate on electrons in this report, because the influence of holes is weak and can be included in a simple, standard way. The basic problem at the evaluation of the drift electron mobility μ at temperatures (500-1000°C) is the determination of scattering mechanisms, which participate in scattering of current carriers. A number of detailed experimental measurements of mobility was performed at low temperatures (50-300K), which can be explained well by scattering of electrons on ionized impurities and polar optical phonons [3]. The influence of ionized impurities on scattering above 400 K is negligible in pure samples and the dominating scattering on longitudinal optical phonons is expected describing μ in the form

$$\mu = \frac{32\varepsilon_0\hbar}{3em}\sqrt{\frac{\pi k_B T}{2m}}\frac{\varepsilon_s\varepsilon_{opt}}{\varepsilon_s - \varepsilon_{opt}}\frac{\exp\frac{\hbar\omega_0}{k_B T} - 1}{\omega_0}\, G\left(\frac{\hbar\omega_0}{k_B T}\right) K\left(\frac{E_g}{k_B T}\right), \qquad (1)$$

where the effective mass $m = 0.096m_0$, the longitudinal optical phonon energy $\hbar\omega_0 = 21.0$ meV, and the optical and static dielectric constants $\varepsilon_{opt} = 7.1$ and $\varepsilon_s = 10.3$ are material parameters. The dimensionless function G is calculated according to Ref. [4] and K describes the correction to nonparabolic conduction band within the Kane model [5]. The mobility is only slightly dependent on ω_0 at high T.

The data of measurements at high temperatures ($T > 500$°C) published so far [6,7] exhibit, however, substantially stronger decrease of μ_H which reaches above 900°C less than one half of its theoretical prediction [8]. Furthermore values from Ref. [7] are $\approx 20\%$ lower

than those of Ref. [6]. The verification of the experimental data and the explanations of the effect is the main topic of this report.

Our measurements of Hall coefficient R_H and electric conductivity σ confirm the reliability of values published in Ref. [7] (see Fig. 2).

There are two recommendations found in the literature to explain the fast decrease of μ_H. The first one [6] expects a strong temperature dependence of material parameters, particularly the static dielectric constant. In agreement with Ref. [8] we do not approve such explanation. In view of (1) and the values of the material parameters, ε_s would have to increase twice within the temperature interval 300°C – 1000°C. Such behaviour of ε_s is not observed in semiconductors. Also in case of ε_{opt} and m their temperature evolution act probably more to the higher than to the lower μ_H.

The second model explanation is based on an assumption of multivalley conduction which comprises both Γ_{1c} minimum and four L_{1c} minima of the Brillouine zone [9]. The heavier electrons in the L-minima reduce μ_H comparing to μ_Γ of pure Γ-valley electrons. The similarity to the same effect in GaAs suggests that the Γ_{1c} to L_{1c} separation ΔE may be much less than $\sim$1 eV which is obtained by band structure calculations [10,11]. Though the idea is known for a long time, there is no concrete calculation of the high-temperature transport in CT except the numerical modeling of the Gunn effect and hot-electron phenomena [12,13]. We mean in this report to complete the knowledge about CT in this respect calculating the electron mobility in the Γ_{1c}-valley μ_Γ and L_{1c}-valleys μ_L, as well as the total Hall mobility μ_H at high temperature including the Γ_{1c}+L_{1c} intervalley scattering and multivalley conduction.

Our treatment is based on the solution of the Boltzmann transport equation within the relaxation time approximation. The polar optical phonon (PO) and acoustic phonon (AC) as dominant intravalley and intervalley scatterings [12] are used. Due to the intention to study transport at high T, this approach can be applied also for the optical phonon scattering. To reduce the amount of unknown parameters all valleys are assumed spherical. The corresponding relaxation times τ_{PO} for polar scattering and τ_{AC} for accoustic scattering read

$$\tau_{PO}(E) = \frac{2\pi\varepsilon_0}{e^2\frac{\partial\Delta k}{\partial E}}\frac{\varepsilon_s\varepsilon_{opt}}{\varepsilon_s-\varepsilon_{opt}}\frac{\exp\frac{\hbar\omega_0}{k_BT}-1}{\omega_0}\,G\left(\frac{\hbar\omega_0}{k_BT}\right), \tag{2}$$

$$\tau_{AC}(E) = \frac{\hbar c_l}{\pi E_1^2 k_B T D(E)}, \tag{3}$$

where Δk expresses the single valley dispersion, $c_l = 7\times10^{10}$ Nm^{-2} is the longitudinal elastic constant [14], and $D = D_\Gamma + 4D_L$ is the total conduction band density of states formed by the single Γ and four L valleys, as well. The intervalley deformation potential is not known in CT, thus we use the intravalley value $E_1 = 4eV$ [14]. This is also the reason why we do not involve other types of scattering into the calculations. Comparing to the uncertainty of the used material parameters such an effort would not provide credible improvement of the results. The function G in (2) expresses the correction to inelastic PO scattering. It allows to use τ_{PO} also at lower temperature where $k_BT \sim \hbar\omega_0$. However, such τ_{PO} produces at low T only approximate Hall factor r_H. The intravalley τ_{PO} can be completed by the intervalley PO scattering terms

$$\tau'_{PO,\Gamma}(E) = \frac{\tau_D}{4D_L(E)} \tag{4}$$

$$\tau'_{PO,L}(E) = \frac{2\tau_D}{2D_\Gamma(E)+3D_L(E)} \tag{5}$$

$$\tau_D = \frac{3\pi\varepsilon_0\hbar}{4e^2k_BTa^2}\frac{\varepsilon_s\varepsilon_{opt}}{\varepsilon_s-\varepsilon_{opt}},$$

which yield the relaxation time comparable with τ_{AC}. The k-space intervalley separation is involved through lattice constant $a = 6.48\mathring{A}$. The total relaxation time for all valleys is given as

$$\tau^{-1} = \sum_i \tau_i^{-1}, \tag{6}$$

where τ_i label all relevant scatterings (2)–(5) which yields the Γ and L mobilities. The Hall mobility μ_H is then obtained in the form

$$\mu_H = \frac{r_\Gamma\mu_\Gamma^2 n_\Gamma + r_L\mu_L^2 n_L - r_p\mu_p^2 p}{\mu_\Gamma n_\Gamma + \mu_L n_L + \mu_p p}, \tag{7}$$

where r_Γ, r_L, and r_p are the Hall factors $< \tau^2 > / < \tau >^2$ and n_Γ, n_L, and p are respective electron and hole concentrations, which are obtained in an obvious way. We found that the fit quality is not influenced significantly by a choice of m_L. We use $m_L = 0.35 m_0$ in this report. This value was successfully used in numerical simulations of the Gunn effect [12].

B. Results and discussion

The valley separation ΔE is fit to the experimental data. We analyze temperature dependent $\Delta E = \Delta E_0 + \alpha T$ which results to the best fit in the form

$$\Delta E = 0.29 - 10^{-4} T(K) \ \ (eV), \tag{8}$$

The results of the calculations together with experimental data are presented in Fig. 2. We see that eq. (8) describes experimental data quite well. For an estimation of the influence of ΔE to μ_H, the theoretical data for a constant ΔE=0.19 eV are shown by the dotted line in Fig. 2. If we consider possible deviations of material parameters and experimental errors, we estimate the precision of our fit of ΔE_0 to $\pm$0.05 eV. The T-independent ΔE produces worse fit with a deviation from the experiment about three times greater than the fit with T-dependent ΔE. Within the estimated experimental precision we cannot, however, confirm $\alpha < 0$ definitely. The $\alpha = 0$ produces the fit which expresses the basic character of $\mu_H(T)$ as well. On the other way, $\alpha > 0$ results in the fit with significant deviations from experiment.

For a comparison, μ_H with L-valley excluded is plotted in Fig. 2, too. In Ref. [7], the drift mobility from the Hall mobility using acoustic-phonon Hall factor $3\pi/8$ was obtained. In view of our Hall mobility presentation we multiplied the data of [7] by that value to return to μ_H here. Numerical simulation of the Gunn effect [12] were performed with ΔE=0.51 eV and $m_L = 0.35 m_0$. This ΔE is however too high to explain our transport data. For a comparison ΔE=0.3 eV and $m_L = 0.22 m_0$ are used in GaAs. The value of α in eq.(8) looks reasonable in respect to the energy gap [15]

$$E_G = 1.622 - 3.5 \times 10^{-4} T - 1.1 \times 10^{-7} T^2 \ \ (eV). \tag{9}$$

The related ellipsometry measurements and theoretical calculations of α due to thermal expansion and life-time broadening were reported for GaAs [16]. The results show that α should be negative in GaAs as well, especially due to the life-time broadening effect.

The effect of the multivalley conduction and the intervalley scattering is demonstrated in Fig. 3. We can distinguish two effects, which reduce μ_H comparing to the single Γ-valley transport represented by the line (a). The electrons in the Γ-valley at the energy above ΔE scatter strongly into L-valleys due to the high density of states there. If these high energy levels are occupied, the mobility μ_Γ is depressed. Such a phenomenon is represented by the line (b). The heavy electrons in the L-valley, shown by line (d), are less mobile but their concentration quickly increases at high T. Finally, due to the stronger effect of transport in the L-valley to the denominator than to numerator in (7), the total Hall mobility drops to its final shape as the line (c).

The involvement of the Hall factors in (7) influences μ_H significantly. As it is shown in Fig. 3, due to the intervalley scattering the relaxation time is reduced at energy above ΔE which results in the increased r_Γ.

IV. HIGH TEMPERATURE DEFECT STRUCTURE - SOLID STATE

A number of galvanomagnetic (GM) measurements performed on samples quenched after annealing under defined pressure of one of the components [15] or in-situ at high temperatures (HT) [6,7,17–19,22,24] exists, which were used to establish equilibrium concentrations of electrically active defects in the region of stability of solid phase. The former method cannot guarantee ideal quenching. Due to a low emission of radiation at lower temperatures and a low heat conductivity of CdTe only a surface layer of samples is cooled quickly and a concentration gradient from surface to the middle of the sample is formed. At high temperatures the emission of radiation and therefore also the cooling is quicker, but as a result of the high diffusion coefficient of Cd the quenched room temperature concentration can correspond to a unknown lower than expected annealing temperature. In the case of

all in-situ measurements published so far the electroneutrality condition (ENC) which was used for high temperature (HT) equilibrium of defects and the interpretation of obtained values of the Hall coefficient R_H and conductivity σ were, however not correct.

We calculate the HT electron transport properties for CdTe with respect to the combined transport both in Γ_{1c} and in L_{1c} space. The nonparabolic **kp** band approximation within the Kane model is used for Γ_{1c} minimum with the effective mass $m_\Gamma = 0.096m_0$ [30]. The band structure near the L_{1c} point is not known precisely. We use parabolic band with effective mass $m_L = 0.35m_0$ here and the Γ_{1c}–L_{1c} valley separation $\Delta E = 0.29 - 10^{-4}T(K)$(eV), which was obtained from the fit of experimental high temperature mobility [57].

Calculation of hole transport properties is more simple, when mostly heavy holes with effective mass m_h=0.83m_0 [11] participate in the transport.

The conductivity σ and Hall coefficient R_H are given by

$$\sigma = e\left(\mu_\Gamma n_\Gamma + \mu_L n_L + \mu_h h\right), \tag{10}$$

$$R_H = \frac{-r_\Gamma \mu_\Gamma^2 n_\Gamma - r_L \mu_L^2 n_L + r_h \mu_h^2 h}{e\left(\mu_\Gamma n_\Gamma + \mu_L n_L + \mu_h h\right)^2}, \tag{11}$$

where r_Γ, r_L, r_h, μ_Γ, μ_L, μ_h, n_Γ, n_L and h are Γ and L electrons and hole Hall factors, mobilities and concentrations, respectively.

The longitudinal polar optical and acoustical modes are expected as a dominant electron and hole scattering mechanisms. The Boltzmann equation is solved using intraband scattering and interband scattering between Γ and four L minima as well. Matrix scattering elements from Nag [14] were used in the calculation.

The following values of material parameters were used in transport calculations: dielectric constants $\epsilon_0 = 10.3$, $\epsilon_\infty = 7.1$ and energy of longitudinal optical phonons $\hbar\omega_{LO}$=0.213 eV [11]. The least amount of information is available about the deformation potential of conduction and valence bands ΔE_e and ΔE_h needed to calculate scattering on acoustical phonons. Nag shows for $\Delta E_e = 4eV$ [14] and ΔE_h can be only roughly estimated by a method proposed by Kranzer [32]. We have used $\Delta E_h = 10eV$ in the calculations.

In this paper the final Hall mobility $\mu_H = |R_H\sigma|$ and Hall concentration $n_H = |1/eR_H|$ are calculated and compared with the experiment. The product $|R_H\sigma|$ calculated first for the intrinsic semiconductor together with experimental points is shown in Fig. 3. The essential influence of the L valley transport to μ_H is evident. A critical analysis of interpretation of Smith [6] and Chern [7] HT concentration data was given by Su et al. [28], but mobility data are in both papers correct and are shown in Fig. 2. More detailed information about mobility calculations is in [57]. The concentrations n_H are evident from Figs. 4, 8.

A. Defect Modeling

We briefly outline the statistics of the defects which is used in this paper. The approach and used symbols are the same as in the Berding's paper [26].

The first task to be solved is a decision about dominant native point defects which control the defect statistics. There was a wide discussion whether Te vacancies (V_{Te}) or Cd interstitials (Cd_I) dominate as donor defects. On the contrary measurements of lattice parameters exist [22] indicating that V_{Te} is the dominating donor. We believe, that this deduction is not fully conclusive, because the samples on which the measurement was performed were prepared by quenching from the three phase line at the Cd site of the P-T diagram. It is known, that such samples are not well defined (non ideal casting) and must contain a relatively large amount of Cd precipitates, which can influence the lattice parameters more strongly than V_{Te}. The *ab initio* calculations [1] prefer Cd_I over V_{Te}. The acceptor defects, Cd vacancies (V_{Cd}) are usually reported and the calculation supports such a result, too. The donor-type Te antisite (Te_{Cd}) was proposed in [1]. Its influence is expected to be strong at Te-saturated conditions. Existence of two P-N lines on CT-Cl doped samples [31] was interpreted by this defect.

In the first approach the densities of neutral native defects mentioned above are given by reaction constants [1]

$$\left[Cd_I^X\right] = \frac{n_o\sqrt{T}P_{Cd}}{K}\exp\left[-\frac{1}{k_bT}\left(E(Cd_I)+U(Cd_I)^{vib}\right)+S(Cd_I)^{vib}\right], \qquad (12)$$

$$\left[V_{Cd}^{X}\right] = \frac{K n_o}{\sqrt{T} P_{Cd}} \exp\left[-\frac{1}{k_b T}\left(E(V_{Cd}) + U(V_{Cd})^{vib}\right) + S(V_{Cd})^{vib}\right], \quad (13)$$

$$\left[Te_{Cd}^{X}\right] = \frac{K^2 n_o}{T P_{Cd}^2} \exp\left[-\frac{1}{k_b T}\left(E(Te_{Cd}) + U(Te_{Cd})^{vib}\right) + S(Te_{Cd})^{vib}\right], \quad (14)$$

$$\left[V_{Te}^{X}\right] = \frac{n_o \sqrt{T} P_{Cd}}{K} \exp\left[-\frac{1}{k_b T}\left(E(V_{Te}) + U(V_{Te})^{vib}\right) + S(V_{Te})^{vib}\right]. \quad (15)$$

E is relevant defect formation energy, energy U^{vib} and entropy S^{vib} determine contributions to the vibrational free energy.

$$K = k_b T^3 \left(\frac{m_{Cd} k_b}{2\pi\hbar^2}\right)^{3/2},$$

$n_o = 1.48 \times 10^{22}$ cm^{-3} is the number of unit cells per volume, k_B is the Boltzmann constant and m_{Cd} is the mass of Cd atom. The label X is used for neutral defect overall.

The densities of multiply ionized defects are calculated for acceptors and donors

$$\left[X^{z'}\right] = \left[X^{X}\right] g_{X^{z'}} \exp\left[-\frac{1}{k_b T}(z\mu_F - E_a^1 - ... - E_a^z)\right] \quad (16)$$

$$\left[X^{z\bullet}\right] = \left[X^{X}\right] g_{X^{z\bullet}} \exp\left[-\frac{1}{k_b T}(E_d^1 + ... + E_a^z - z\mu_F)\right], \quad (17)$$

where E_a and E_d are the acceptor and donor one-electron ionization energies and μ_F is the Fermi energy. $g_{X^{z'}}$ ($g_{X^{z\bullet}}$) is the degeneracy of the defect. The index z means the ionization degree, the prime and bullet correspond to negative and positive species. Experimentally determined ionization energies of native defects are shown in Tab.1. Important are especially deep donor levels for V_{Cd} and acceptor levels for V_{Te}. These results were obtained from EPR measurements, one of the most precise and reliable methods for a determination of activation energies of defects. The values of energies and entropies established by theoretical calculations for defects are given in the Tab.2. Based on the given forms, the *ab initio* calculations describe the properties of native defects in CT qualitatively [1]. The relations (16),(17) present a simplified statistical model. The exact relations (see e.g. [33]) yield only slightly different results. The deviations from the experimental data are however too extensive to describe the relevant quantities in a practically applicable form. In this respect we suggest a variant (semiempirical) approach in this paper to solve the task of native defects

in CT. We fit the experimental high-temperature σ and R_H optimizing key parameters of the *ab initio* output (formation energy, vibration free energy) by parameters to hit the native defects properties in CT more satisfactorily. Henceforward we use donor-type (Cd_i and Te_{Cd}) and one acceptor-type native defect (V_{Cd}). The donors are described by (12) and (14) and the acceptor is described by (13). The set of native defect ionization energies and degeneracy factors which are used in the calculations is collected in Table 1. The Fermi energy is obtained solving electric neutrality condition in which Γ and L electrons, holes and singly and doubly ionized native defects are included.

$$n_L + n_\Gamma + [V'_{Cd}] + 2\,[V''_{Cd}] = p + [Cd_i^{\cdot}] + 2\,[Cd_i^{\cdot\cdot}] + [Te_{Cd}^{\cdot}] + 2\,[Te_{Cd}^{\cdot\cdot}] \tag{18}$$

Comparison of concentrations of defects calculated with the help of eqs. (12,13,14,15) shows, that Cd vacancies V_{Cd} play the dominant role as acceptors and Cd interstitials as donors. The tellurium antisites Te_{Cd} can have a smaller influence as donors. The impact of Te vacancies is negligible.

B. Results and discussion

The same band parameters from III.A which fit the Hall mobility $\mu_H = |R_H\sigma|$ were consecutively used for the modeling of native defects. The electric neutrality condition and the Boltzmann equation were solved. The theoretical and experimental value of $n_H = |1/eR_H|$ are plotted in Fig. 4. It is necessary to bear in mind that n_H in the case of occupied L-band does not express the electron concentration. Measurements performed under Cd pressure (full points) exhibit a good agreement with the experiment. On the contrary the discrepancy between theoretical values and experimental data of measurements done under Te pressure (open points) is slightly larger probably due to a higher influence of Te on a quality of Mo welded contacts. For all experimental points $R_H < 0$. Corresponding experimental and theoretical values of conductivity σ in dependence on Cd or Te pressures at different temperatures are shown in Fig. 5.

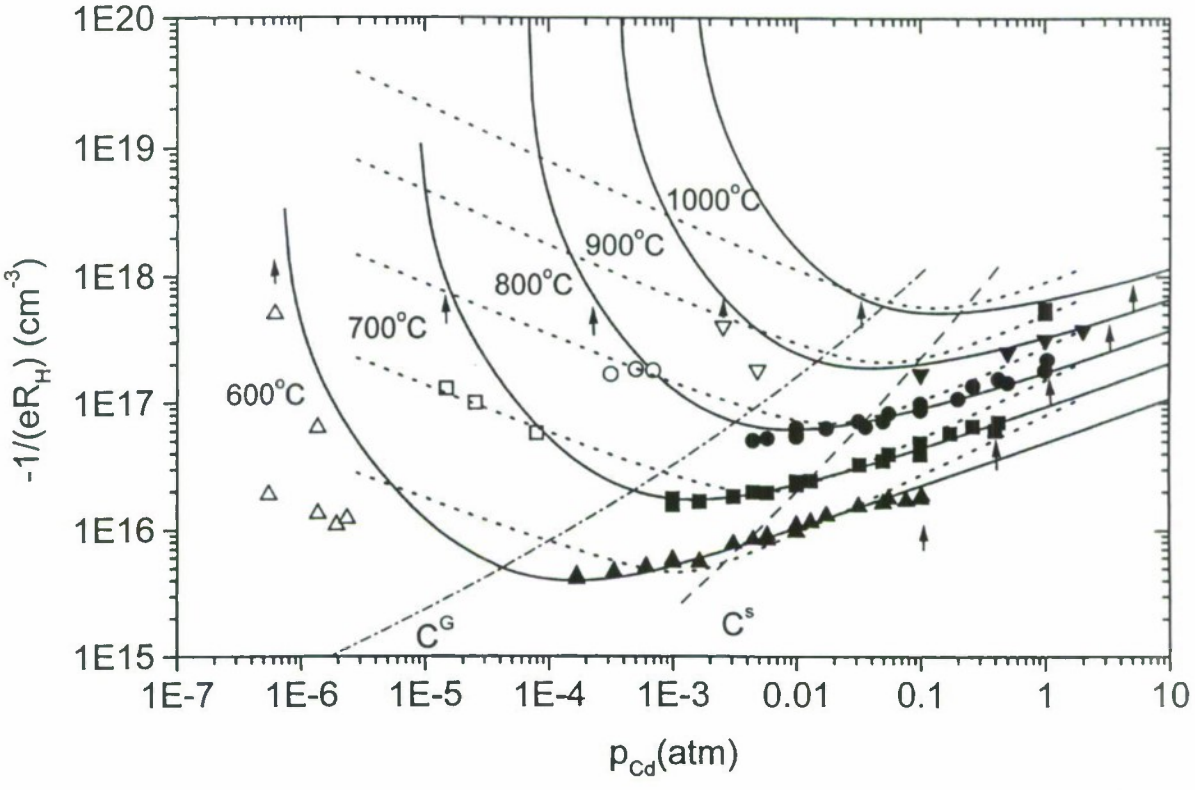

Fig.4. The experimental (upper triangles – 600°C, squares – 700°C, circles – 800°C, bottom triangles – 900°C and squares – 1000°C) and theoretical Hall concentrations. The full lines show the fit within presented model. The dotted lines are results when the Te_{Cd} was included in the model. The dash line outlines the position of the stoichiometric (P–N) line which was obtained from the theoretical calculations based on the presented model. The dash-dot line shows the position of the line of congruent sublimation. The arrows show the Cd saturation limit.

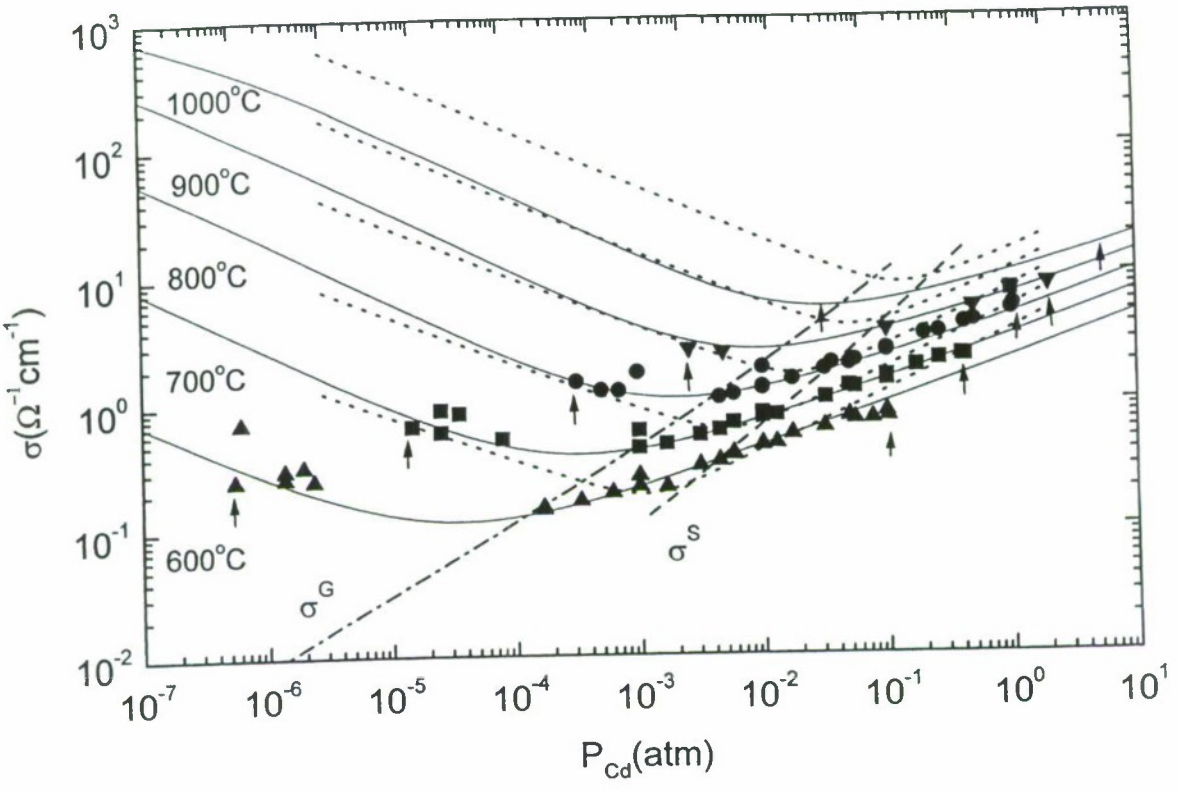

Fig.5. The experimental (upper triangles – 600°C, squares – 700°C, circles – 800°C, bottom triangles – 900°C and squares – 1000°C) and theoretical conductivity. The full lines show the fit within presented model. The dotted lines are results when the Te_{Cd} was included in the model. The dash line outlines the position of the stoichiometric (P–N) line which was obtained from the theoretical calculations based on the presented model. The dash-dot line shows the position of the line of congruent sublimation. The arrows show the Cd saturation limit.

The fitted donor and acceptor energies and entropies together with the *ab initio* results [1,26] are shown in Table 2. We present total formation+vibration energies only because the E and U^{vib} cannot be distinguished in the fit. The agreement of theoretical and experimental values is very good.

The effect of Te antisite Te_{Cd} cannot be estimated within our model definitely. From the point of view of the HT properties at the Te saturate conditions, where Te_{Cd} should play the most significant role, we observe a strong influence of the hole transport, which results in the decrease of the Hall mobility in this region. Due to the low mobility, however, the holes do not revert the sign of R_H which stays negative. The donor Te_{Cd} compensates acceptor V_{Cd} keeping the electron high-mobility transport dominating at the Te saturation as well. Such a behaviour is evidently not observed within all temperature interval where the measurements at the Te saturated side were performed. We can thus deduce that Te_{Cd} is a minor defect above 600°C and does not manifest in the electrical measurements. The real concentration of charged Te_{Cd} is less than some limit value which prevents Te_{Cd} to prevail. We have estimated such a value within the parameters in Tables 1. a 2. by a value E >6 eV which is to be substituted in the Eq. (14). The open question remains the concentration of the neutral Te_{Cd}. The ionization energy used in our calculation is not set safely and the model of Te_{Cd} as a deep donor can be valid as well. In such a case the concentration of neutral Te_{Cd} could increase significantly without the effect to the electrical measurements but having an impression to the solidus curve in the T-x diagram.

The essential effect of the four L minima in the conduction band to the native defect statistics is outlined in Figs. 6, 7, 8, 9, 10 at 800°C. Due to the occupation of the L bands the relevant electron concentration is not expressed satisfactorily by $|1/eR_H|$. If higher minima in the band structure are occupied, the simultaneous analysis of both R_H and σ describes the carrier concentrations and mobilities correctly. Consequently the concentration of native defects can be twice or more higher than electrons being assumed only in the Γ-point. The dash line shows the concentration of electrons and holes at room temperature.

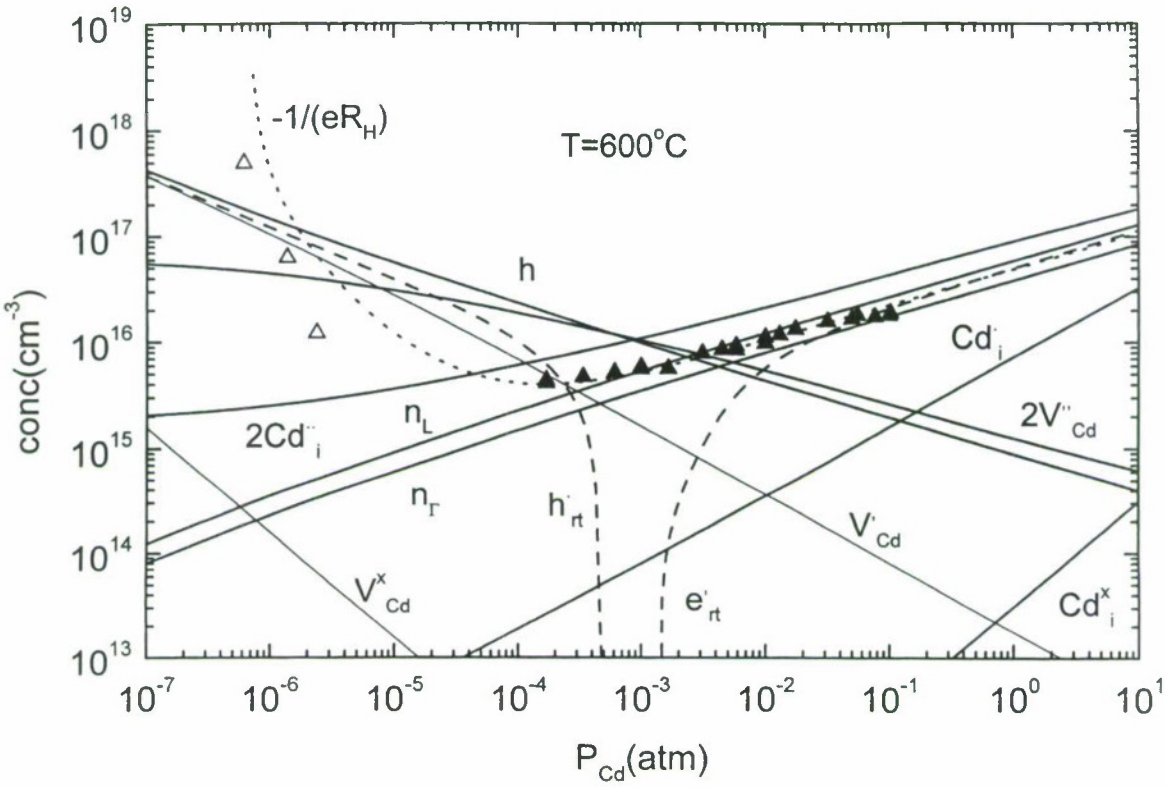

Fig.6. The neutral (x) and ionized (' ; •) native defect concentrations together with total electron (e') and hole (h•) concentration, all at 600°C, are plotted by full lines. The experimental (squares) and theoretical (dotted) $|1/eR_H|$ identical with that in Fig. 4 are involved. The dash lines show room temperature e' and h•.

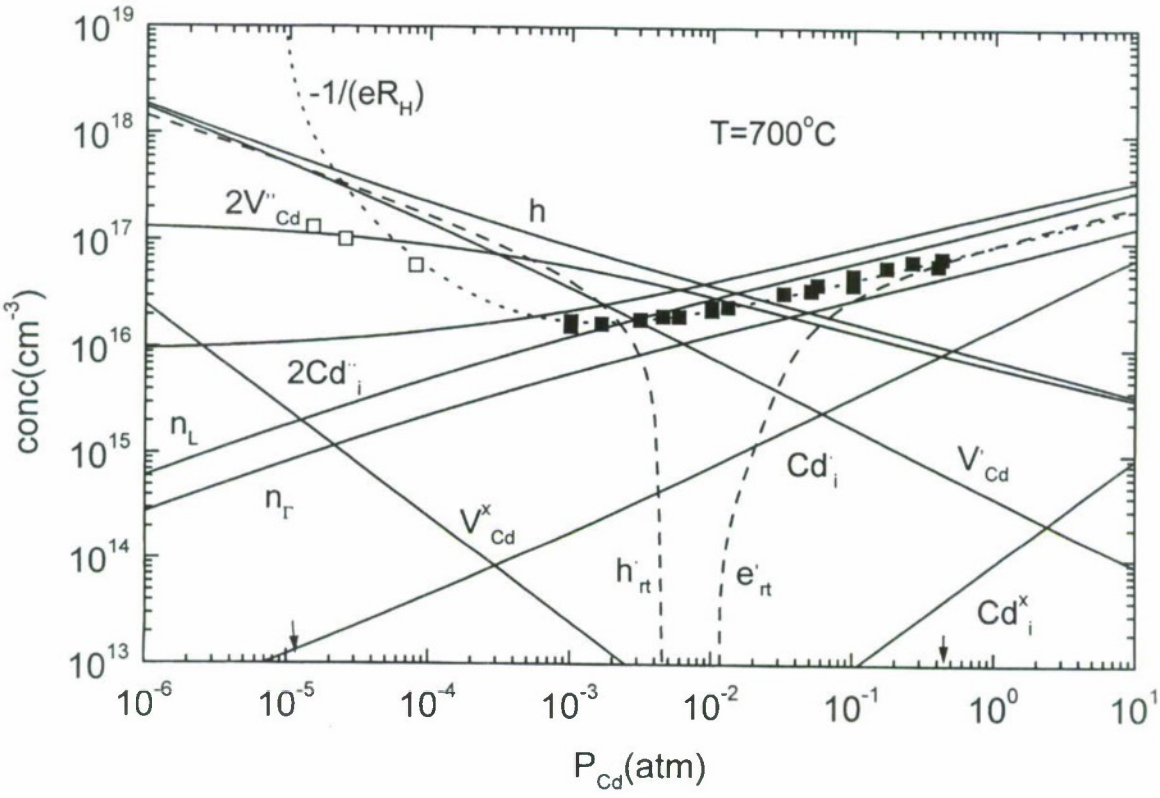

Fig.7. The neutral (x) and ionized (' ; •) native defect concentrations together with total electron (e') and hole (h•) concentration, all at 700°C, are plotted by full lines. The experimental (squares) and theoretical (dotted) $|1/eR_H|$ identical with that in Fig. 4 are involved. The dash lines show room temperature e' and h•.

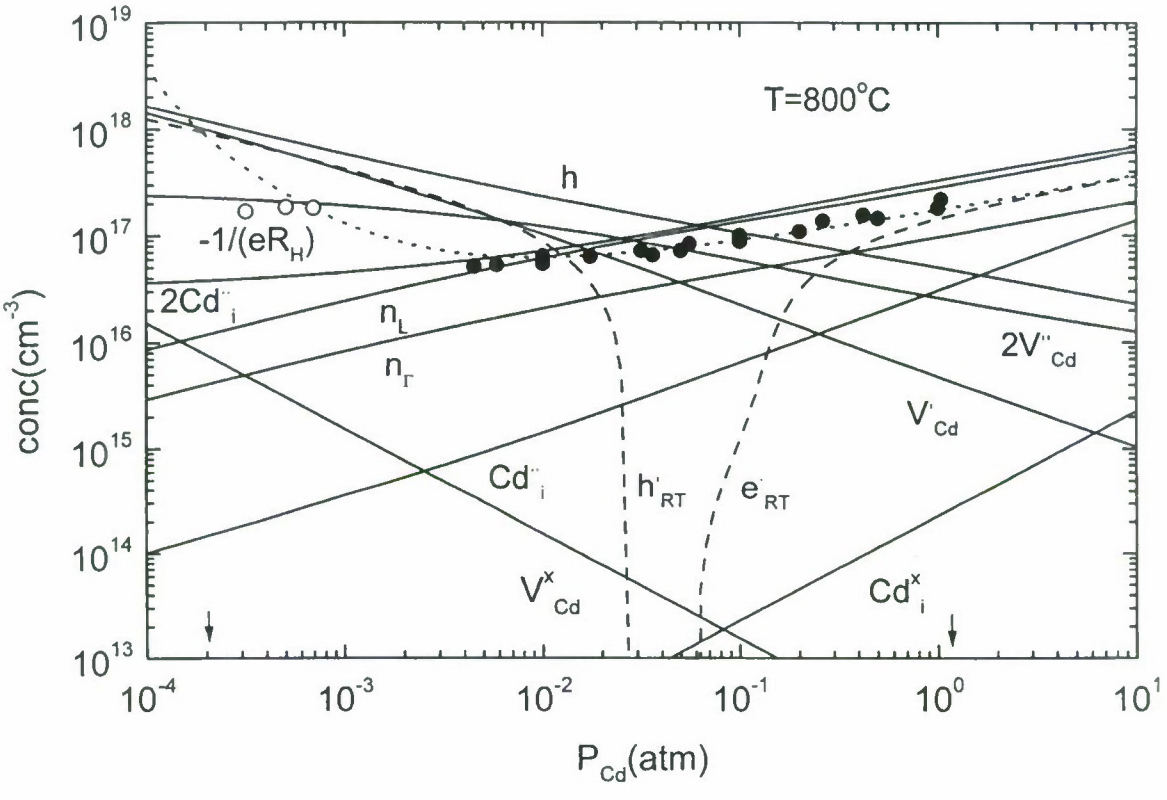

Fig.8. The neutral (x) and ionized (' ; •) native defect concentrations together with total electron (e') and hole (h•) concentration, all at 800°C, are plotted by full lines. The experimental (squares) and theoretical (dotted) $|1/eR_H|$ identical with that in Fig. 4 are involved. The dash lines show room temperature e' and h•.

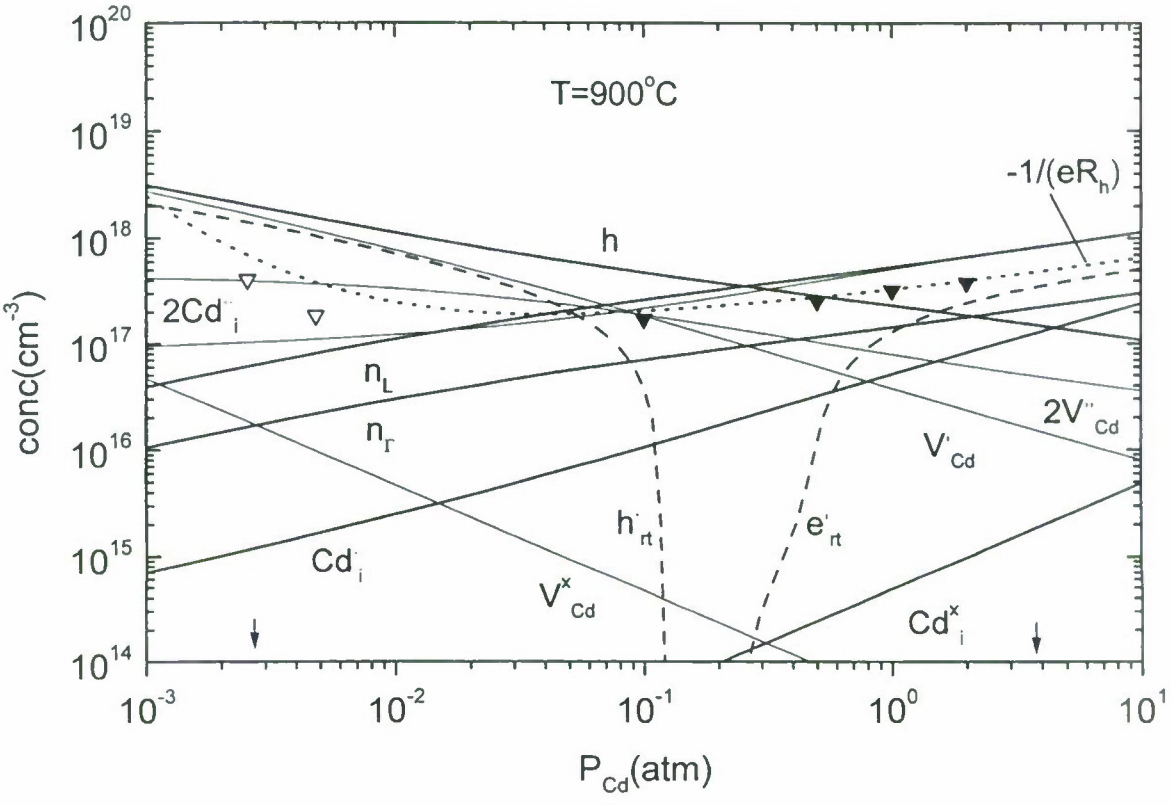

Fig.9. The neutral (x) and ionized (' ; •) native defect concentrations together with total electron (e') and hole (h•) concentration, all at 900°C, are plotted by full lines. The experimental (squares) and theoretical (dotted) $|1/eR_H|$ identical with that in Fig. 4 are involved. The dash lines show room temperature e' and h•.

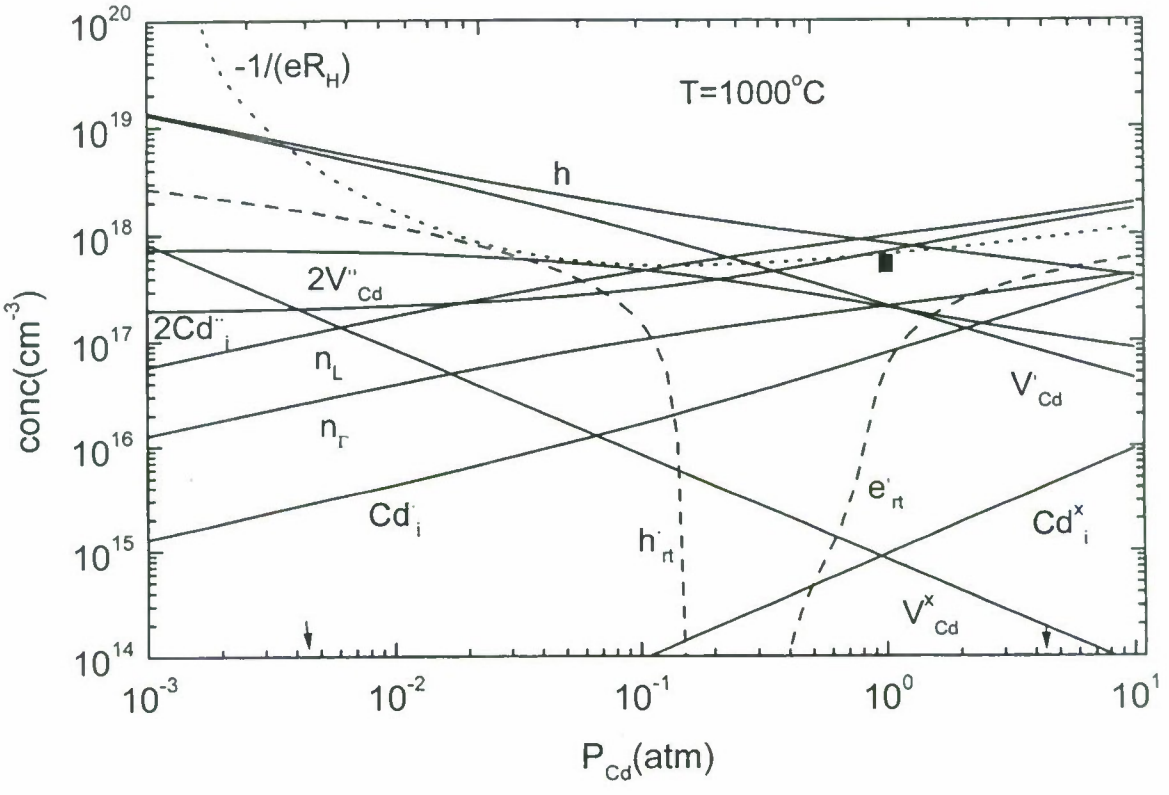

Fig.10. The neutral (x) and ionized (' ; •) native defect concentrations together with total electron (e') and hole (h•) concentration, all at 1000°C, are plotted by full lines. The experimental (squares) and theoretical (dotted) $|1/eR_H|$ identical with that in Fig. 4 are involved. The dash lines show room temperature e' and h•.

The knowledge of equilibrium concentrations of defects at HT allows to establish the crystal properties at 300K, which are essential for technological applications, when usually crystals with a minimum deviation from stoichiometry are demanded. If the concentrations of defects at HT are known and we suppose an ideal quenching, we can determine by a solution of electric neutrality condition at 300K isoconcentration lines for electrons n_r and for holes h (n_L is at 300K negligible) in dependence on annealing conditions (T, p_{Cd}), from which the crystal was quenched. Isoconcentration lines are shown in the P-T diagram in Fig. 11. The region of pressures p_{Cd}, at which the Fermi level of the sample at the room temperature is at the same position as it is in the intrinsic semiconductor can be seen in this plot. Corresponding line (the so called P-N line), for which the following expression was found

$$P_{Cd}(P-N) = 4.5 \times 10^5 \exp(-1.73 \times 10^4/T)(atm) \tag{19}$$

is given in Fig. 1. Here also the lines corresponding to stoichiometric composition of gas p^G and liquid p^L are plotted. This P-N line roughly gives conditions for preparation of samples with a minimum deviation from stoichiometry. We verified its position by annealing/quenching experiments at 600^oC, 700^oC, 800^oC, 900^oC under different Cd or Te pressures, when annealing time was chosen high enough to establish equilibrium concentrations of defects by the diffusion process. The obtained results of p_{Cd} are slightly higher than those obtained from evaluation of HT conductivity and Hall effect measurements and are lying within the gray area marked in Fig. 12.

From the point of view of preparation of single crystals with a minimum deviation from stoichiometry it is necessary to know the curve of solidus in the T-x diagram. This can be evaluated from equilibrium concentrations of electrically active defects established from Hall measurements on the three phase line [6,21,22] or directly from thermodynamic measurements of Cd or Te pressure on the three phase line [37,38,43]. Thermodynamic and galvanomagnetic measurement of Cd-rich solidus are not contradictory. A discrepancy existed for the Te-rich solidus,

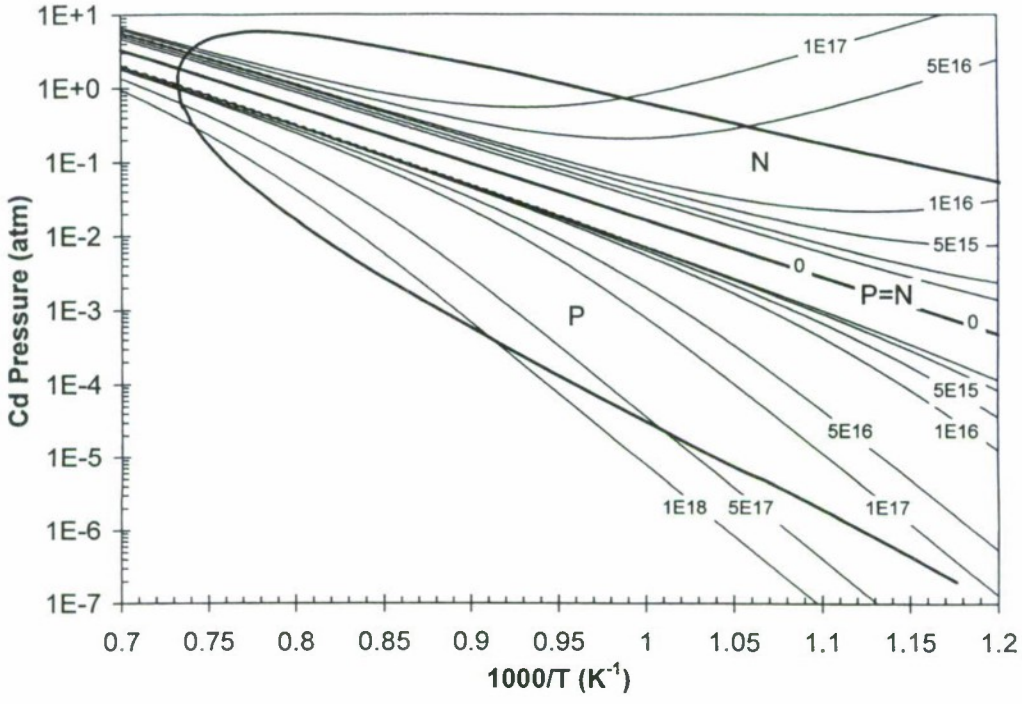

Fig.11. P-T diagram with isoconcentration lines for electrons n_Γ and holes h

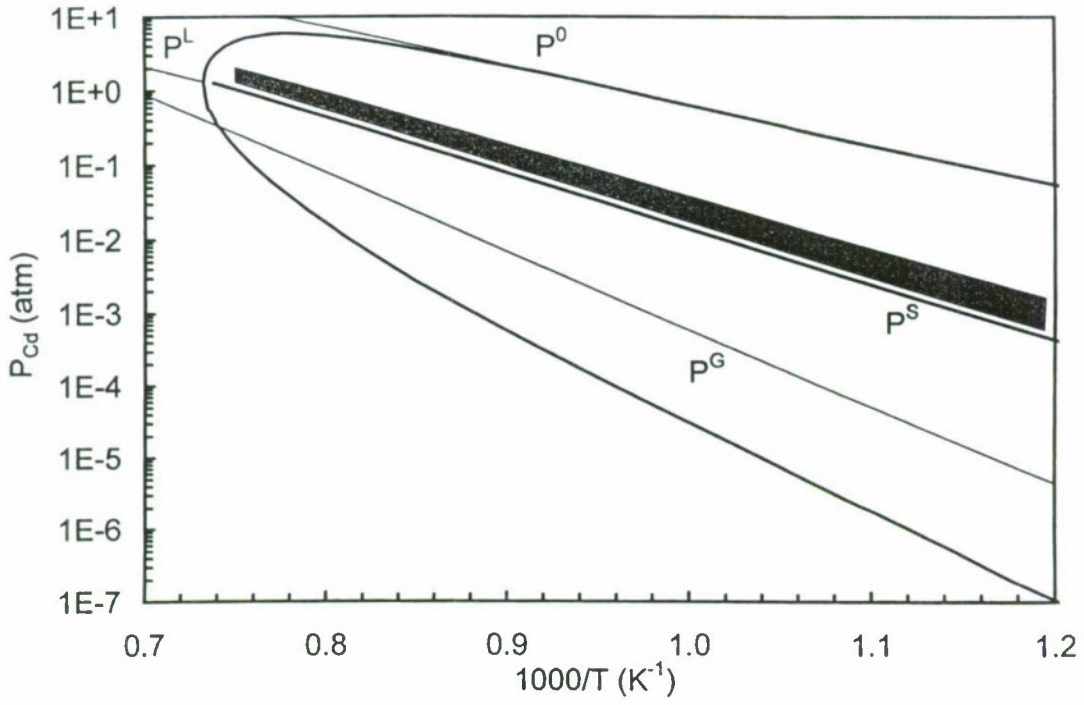

Fig.12. Partial pressure of Cd along the three-phase loop of CdTe(S). The full lines P^S, P^L, and P^G represent the partial pressure over stoichiometric CdTe(S), stoichiometric CdTe(L), and congruently subliming CdTe(S) or evaporating CdTe(L), respectively. The P^S was found based on results of the presented model. The grey area gives the region of approximate position of this line as observed from our annealing and quenching experiments. P^0 is Cd partial pressure over pure Cd.

especially between measurements of R_H [22] and thermodynamic measurements [37,45]. Based on results of our experiments it is possible to establish the solidus curve and compare the obtained results with these experiments. The arrows in Fig. 4 indicate pressures corresponding to the three phase boundary. The solidus curve constructed for these points and for the whole three phase line is shown in Fig. 13. The agreement of our measurements and those of Refs. [37,43,45] both for Cd and Te-rich sides is good. Comparison our results with the results of Wienecke [22], who measured R_H and σ in-situ in dependence of temperature, Cd and Te pressure corresponding to the three phase line yields a good agreement on the Cd rich side. On the contrary a significant discrepancy can be seen on Te-rich samples. The interpretation of measurements of R_H and σ on the Te side of the P-T diagram is incorrect from the following reasons: The assumption, that R_H is not influenced by electrons, if their concentration is roughly one order of magnitude lower than intrinsic concentration, is false. Even due to the fact, that the value of mobility ratio b=$(\mu_e/\mu_h) \sim 10$ in the discussed temperature interval, inversion of sign of R_H should occur at 580°C. The quantity (p-n) cannot be found from measurements in weak magnetic fields without a knowledge of mobilities of electrons μ_e and holes μ_h, which are not given in [22]. The mobility values, which strongly influence the obtained concentrations of defects are not presented in ref. [23] as well.

Further contradictions are apparent. The authors supposed, that the electric neutrality condition p-n=N_A is valid in the whole interval of temperatures. This means, that in this temperature region acceptors N_A are fully ionized. This can be reached only for shallow acceptors. In such a case, however, the slope of temperature dependence of concentration (p-n) determines the energy of formation of V_{Cd}. Using the data of Ref. [22] yields the value 740meV, which is substantially lower than the result of ab initio calculations.

High-temperature *in situ* Hall effect and conductivity measurements are presented in this paper. The results show, that at high temperatures two types of electrons participate in the transport: Electrons in the Γ point with $m_\Gamma = 0.096 m_0$ and electrons in the L point with $m_L = 0.35 m_0$. New experimental values of energy and entropy terms of native point defects in CdTe are presented and comparison with the *ab initio* calculations show a good

agreement. The position of isoconcentration lines for electrons and holes, P-N line in the P-T diagram and the solidus line in the T-x diagram, which describe well the experimental data were established. The dominant preference of the reported research is comprised in the integral description of various features of CdTe within the only one model. The most of the parameters which are used were obtained from the independent experiments and the fit of several of them do not deviates significantly from their theoretical predictions.

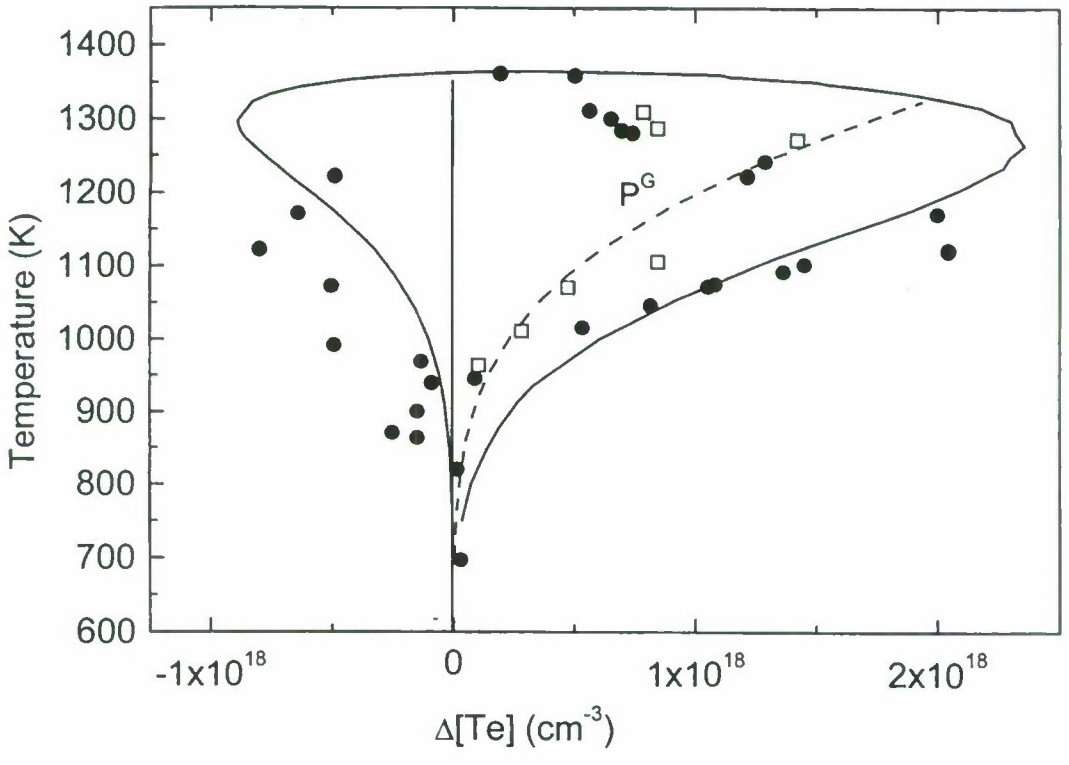

Fig.13. Tellurium atom concentration in CdTe for Cd and Te - saturated conditions. Circles represent experimental data from Ref. [38] and squares data from ref. [37]. The dash line plots the gasus stoichiometry conditions.

V. GALVANOMAGNETIC PROPERTIES BELOW AND ABOVE THE MELTING POINT

To prepare high quality single crystalline CdTe from the melt, it is necessary to have sufficient information on the S-L-G phase equilibrium and on the L-G and S-G equilibria. The phase equilibrium S-L-G was studied experimentally both on the Cd side [15,42–44] and the Te side [44,45] and theoretically [1]. The phase equilibrium S-G is relatively well known from conductivity and Hall effect measurements in dependence on temperature and pressure of one of the components, which were mainly used to study the S-G equilibrium experimentally [15,6,7,22]. Due to the fact, that multivalley transport of electrons has to be taken into account (see section III), a new interpretation of Hall effect and conductivity experimental data received so far was performed(Section IV). The least amount of information is available about the L-G equilibrium above the melting point. The equilibrium pressure of Cd gas over the liquid characterizing the stoichiometric composition of the melt is shown in the p-T diagram in Ref. [46]. Usually three species are assumed in liquid phase: Cd and Te atoms and CdTe molecules. This assumption was not proved experimentally. Our growth experiments performed by gradual cooling of the melt in the temperature gradient show, that the quality of the crystal can be closely connected to the history of the CdTe melt. Therefore the fabrication of high quality CdTe crystals represents a very complex technological problem in comparison to crystals of elementary or III-V semiconductors.

The study of the CdTe liquid is interesting also because it embodies an extremely different behaviour which differs from the liquid of group IV and III-V semiconductors. The basic difference reposes on the fact, that strong cohesive forces remain after the destruction of long-range order and that a liquid model with weak interactions is inappropriate in CdTe in comparison to e.g. GaAs [47]. Measurements of neutron diffraction [48] confirm the existence of the short-range ordered network. This fact is confirmed also by other experiments performed in liquid CdTe. It was observed [49,54], that the dependence of the electrical conductivity on temperature in the liquid CdTe is the same like for semiconductors in the

condensed phase, when the electrical conductivity rises with the increasing temperature. Such a behaviour was not observed experimentally in any semiconductor from group IV or III-V, where the electrical conductivity has a metallic character and the change between the semiconducting and metallic behaviour has a step-like form. Numerical calculations for liquid CdTe [2] show, that metallic behaviour is not typical for CdTe, probably due to the ionicity. A higher ionicity of Cd-Te coupling limits the delocalization of electrons, which can contribute to the semiconducting behaviour of the liquid CdTe.

The measurements of GM properties below and above the melting point were performed in two stages. In the first stage we concentrated on conductivity measurements. Then the measuring cell was modified and improved in order to enable Hall effect measurements.

A. Conductivity

Our DC measurement of electrical conductivity was performed in a quartz cell in the van der Pauw configuration and spectrally pure graphite was used to prepare contacts. The temperature was measured by a Pt-PtRh thermocouple. The cell was connected with a CdTe stack and both were filled by CdTe powder. After melting a free volume in the stack was approx. the same as a volume of the cell. Due to the fact, that it was not possible to control the P_{Cd} overpressure above the sample, both the solid and liquid were weakly depleted of Cd. The depletion of Cd is connected with a change of the concentration of point defects (probably V_{Cd}). The temperature dependence of the conductivity was measured after melting of CdTe up to 1200°C. Subsequently the cooling was performed with the rate 15°C/hour at temperatures 1200-1000°C and with rate 30°C/hour at temperatures 1000-400°C. This process was followed by another heating/cooling cycle between 400 and 1200°C. No significant difference of conductivity between both heating/cooling dependencies was observed. The results of our measurement together with those from Ref. [49,54] are shown in Fig. 14. Two clear slopes can be seen on our line - 0.7 eV in the solid and 4.6 eV in the liquid.

The equilibrium concentrations of defects in the whole region of stability of solid phase depend on the temperature and gas pressure of one of the components. It would be optimum to study the electrical conductivity on a sample, at which the position of the Fermi level is close to the intrinsic Fermi level, it means close to the solidus-stoichiometry-line marked in the p-T diagram (Fig. 15) as P^S. This line is sometimes called the P-N line. Due to the fact, that our measurements were performed in a wide range of temperatures it was possible to compare data obtained at lower temperatures on solid CdTe with our independent in-situ galvanomagnetic measurements which were performed at defined T and P_{Cd} [57]. Based on this comparison we could also complete the P_{Cd} into presented data shown as the points in Fig. 15. The dash line plots a seeming path of the sample through the P-T diagram, along which the measurements were performed. We notice that the limit $P_{Cd} \to 0.0015$ atm at low T is not a real effect but it results from the foreign impurity conduction with a concentration $5 \times 10^{15}\text{cm}^{-3}$ in this sample. The real P_{Cd} ought to follow a line nearly parallel with the gas-stoichiometry-line P^G as it is well expressed at $1000/T < 0.9K^{-1}$ showing a depletion of Cd in the CdTe solid sample. The moderate shift of the points away the P^G at high temperature is probably due to extrapolation error near P^G. Because of a fast sublimation of the sample near P^G no in-situ galvanomagnetic data at defined P_{Cd} are available there and the comparison with the points near P^S was done. The continuation of the experimental P_{Cd} into the liquid was calculated via solution of balance-mass-equations where stoichiometry liquidus pressure line P^L was applied.

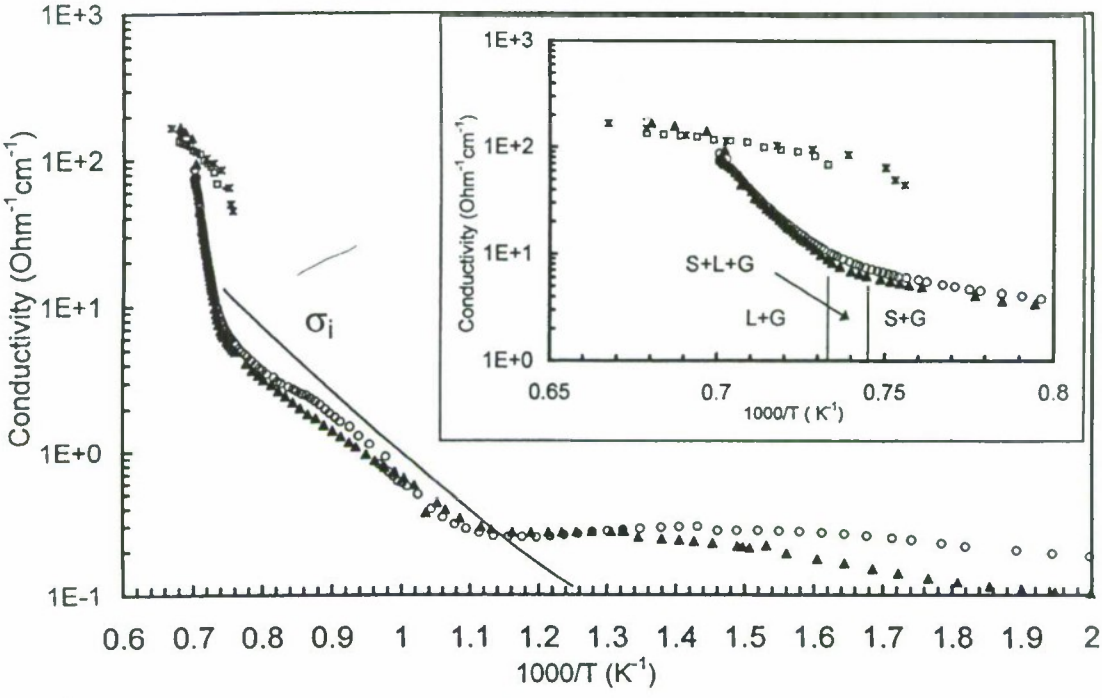

Fig.14. The conductivity of CdTe vs 1000/T. Our results are shown for cooling (full triangles) and heating (open circles), respectively. The measurements of [49] and [54] are included as (stars) and (open squares), respectively. The full line shows theoretical intrinsic electrical conductivity of solid σ_i according to [57]. The labels in the inset point to the solid-gas (S+G) and the liquid-gas (L+G) phase equilibrium, the medium area (S+L+G) corresponds to the three-phase S-L-G equilibrium.

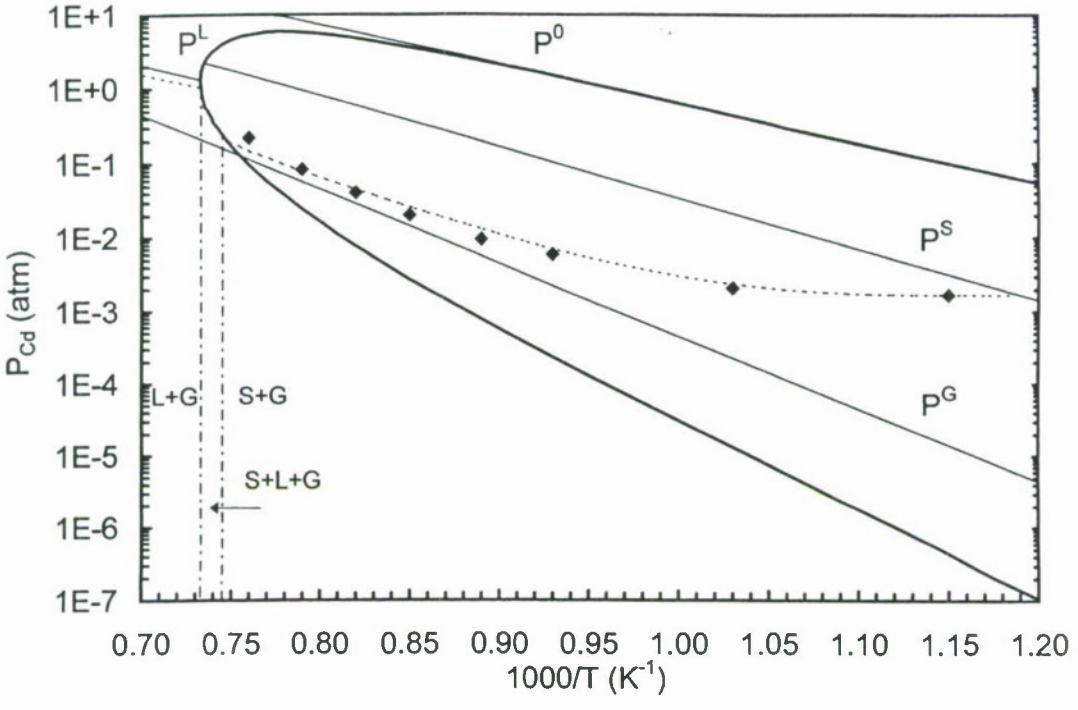

Fig.15. Partial pressure of Cd along the three-phase loop of CdTe(S). The full lines P^S, P^L, and P^G represent the partial pressure over stoichiometric CdTe(S), stoichiometric CdTe(L), and congruently subliming CdTe(S) or evaporating CdTe(L), respectively. P^0 is Cd partial pressure over pure Cd. The full diamonds and dash line plots the experimental path through the region, see details in text. The labels correspond to the previous figure.

The sample starts to melt at $T = 1069°C$ and $P_{Cd} = 0.23$ atm and is completely molten at $T = 1090°C$ and $P_{Cd} = 1.04$ atm. As it can be seen from Fig. 15, the phase transition solid-liquid starts in our case close to the intersection of the P^G line with the three phase boundary. Our experimental value of the electrical conductivity at the melting point is $\approx 10\ \Omega^{-1}cm^{-1}$, the measurements from Ref. [49,54] give 60 $\Omega^{-1}cm^{-1}$ and 90 $\Omega^{-1}cm^{-1}$, respectively. These differences can be explained by the fact, that the measurements [49,54] were probably performed on sample with a larger deviation from stoichiometry, what can be deduced from the lower temperature of the melting point in their measurements. The conductivity below and above the melting point of CdTe were also performed by non-contact EDDY current measurement Ref. [51]. The values of conductivity in the liquid are in good agreement with the results of our measurements. The abrupt increase of conductivity from solid to liquid state in [51] compared to our results can be caused by a smaller deviation from stoichiometry in their sample, due to the minimized free volume in the ampoule. Transition from liquid to solid state in this case occurs close to the maximum melting point at 1092°C.

B. Hall effect

The construction of Hall cell for measurement of Hall effect in liquid CdTe in the Van der Pauw configuration represents a difficult technological problem. The keystone of our construction of the experimental setup is a quartz cell with four pipe outlets for a connection of contacts. It came out, that most metals react with liquid CdTe resulting in a metal dissolution and subsequent strong doping of the liquid. It appeared that only graphite could be used as contacts. We used spectrally pure graphite with purity 5N. Both DC and AC methods were used to measure σ and R_H. It appeared, that the latter is more suitable especially for measurements above the melting point due to reduced noise. These measurements were performed in a DC magnetic field, when AC current with frequency 600Hz was passing through the sample. The measuring cell connected with a stack was evacuated and completely filled with liquid CdTe after heating above the melting point

temperature. Several measurements of transitions from solid to liquid and back with both increasing and decreasing temperature were done. The goal was to measure the temperature dependence not only around the melting point, but also in a wide range of temperatures (600-1250°C) in order to compare the obtained values of Hall coefficient R_H with data from measurements on crystalline CT at temperatures (600-1000°C). The measurement was performed in a one zone furnace, when the temperature was measured and controlled by a Pt-PtRh(10%) thermocouple. The cell and the stack had almost the same temperature. Due to the complexity of construction of the measuring cell it was not possible to maintain defined pressure of one of the components above the solid and liquid during the measurements. Some free volume existed above both the solid and liquid sample, in which CdTe dissociated to components Cd and Te_2 existed in gas phase. The state of binary CdTe existing in two phases (S-L and L-G) is according to the Gibbs' phase rule determined by temperature and pressure of one of the components above the solid or liquid, only on three phase line (S-L-G) by temperature. Concretely R_H and σ depend on temperature and p_{Cd} pressure in the region of stability of the solid and only on temperature on the three phase line.

In our case the more volatile component - Cd starts to leave the material until the Cd pressure p_{Cd} reaches the values close to the line of congruent sublimation.

The temperature dependence of $1/(eR_H)$ is shown in Fig. 16. The arrow indicates the value corresponding to the melting point. The sign of R_H is negative both below and above the melting point. The temperature dependence of electrical conductivity and Hall mobility is given on Figs. 17 and 18, where the melting point is again indicated by an arrow. The measurement in the solid state was analyzed by the way described in the preceding sections.

The supposed conditions of experiment under which the measurement from low temperature (600°C) to the melting point (1092°C) or back were performed are very close

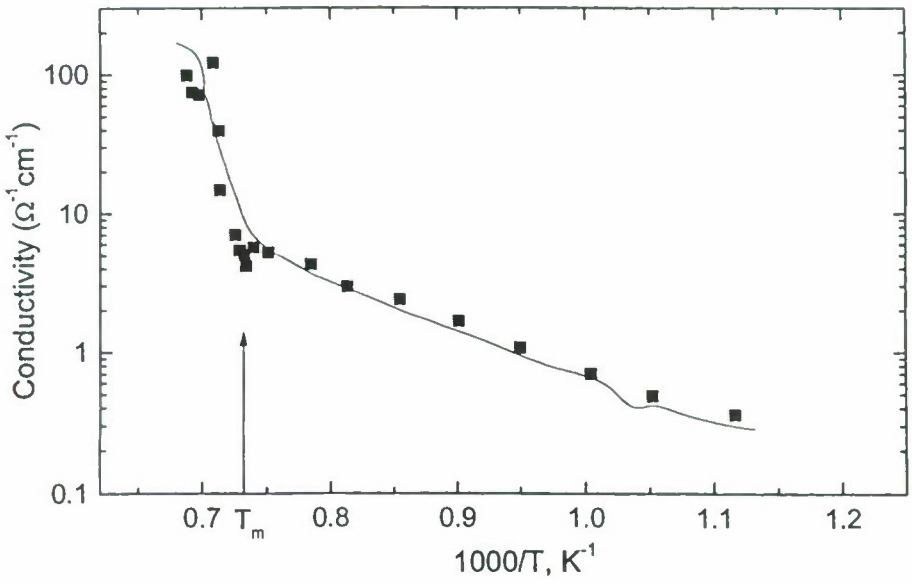

Fig.16. The conductivity below and above the melting point of CdTe. The arrow indicates the temperature of the melting point.

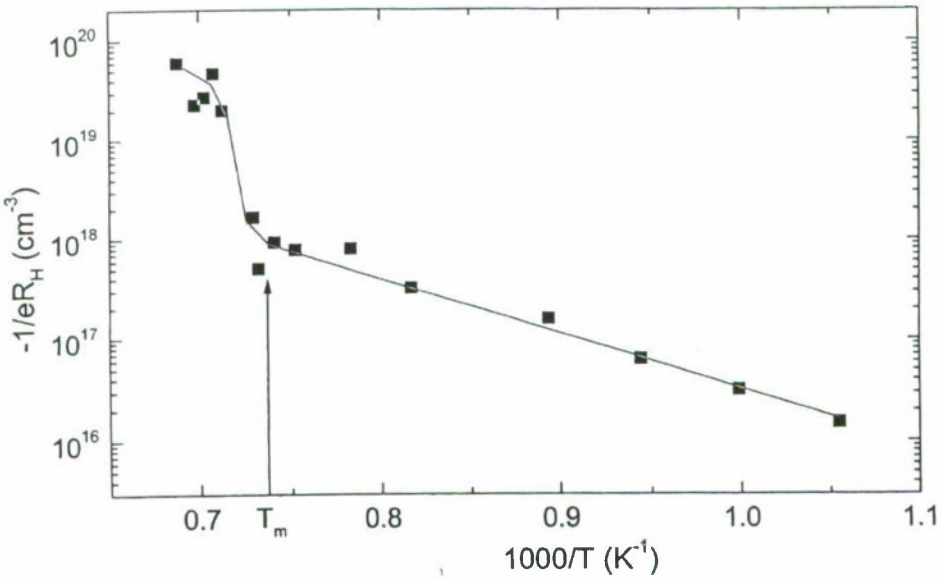

Fig.17. The $1/(eR_H)$ below and above the melting point of CdTe. The arrow indicates the temperature of the melting point.

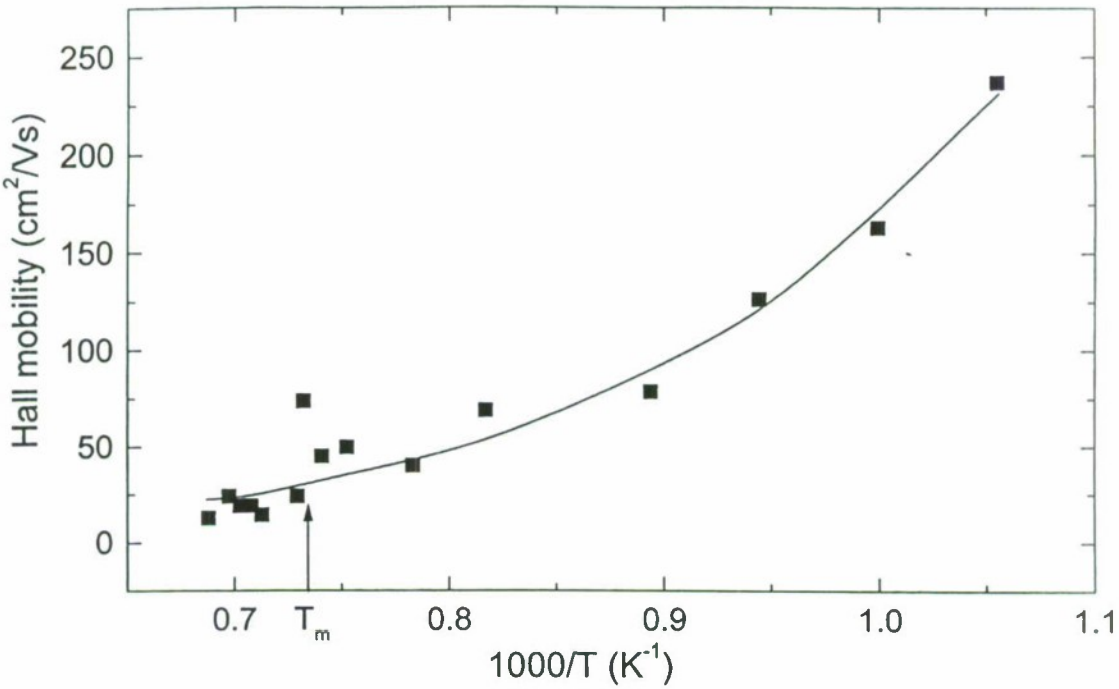

Fig.18. The Hall mobility below and above the melting point of CdTe. The arrow indicates the temperature of the melting point.

to those discussed for the experiment, when only conductivity was measured (Fig. 15).

C. Discussion

To elucidate the interesting properties of the liquid CdTe, we suggest a model explanation which describes the observed experimental data. It needs, however, a detailed and critical discussion and also more extended experimental basis to be verified satisfactorily.

We discern three temperature intervals of the existence of the liquid with a distinct thermodynamic or electric behaviour. The first interval ($1069°C < T < 1090°C$) corresponds to the melting. The three phases solid-liquid-gas exist simultaneously. The P_{Cd} strongly increases and the sample is significantly enriched by Te from $\sim 10^{18}\text{cm}^{-3}$ at the lower T to $\sim 10^{20}\text{cm}^{-3}$ at the upper limit T. Simultaneously, the conductivity is not substantially influenced by that. This means that Te is not our electrically active species here.

In the second interval ($1090°C < T < 1160°C$) the CdTe is fully molten. The escape of Cd from the sample stops. The liquid behaves continuously as a semiconductor with a highly thermally activated free electron concentration. We interpret the strong increase of σ characterized by the energy 4.6 eV as a formation of electrically active Cd. We expect that the short-range ordered medium coexists with randomly distributed Cd and Te atoms. In the ordered form, the covalent binding between II-VI compounds survives resulting in the semiconductor-like behaviour. The disordered atoms can be regarded as defects in the lattice being both donor- and acceptor- like, generally. From point of view of the most frequently used electrically active native defects in the solid, which are Cd interstitial Cd_I and Cd vacancy V_{Cd}, we recommend to describe the process to be a dissociation of the ordered liquid CdTe according to the reaction

$$CdTe \rightarrow TeV_{Cd} + Cd_I, \tag{20}$$

where the final products are the vacancy in the correlated ordered lattice V_{Cd} and free unbound Cd_I. The observed slope in σ and R_H is in a good agreement with first-principle calculation of this energy in the solid which comes out 4.2 eV [1].

While Cd_I is the electrically active divalent donor, the V_{Cd} in the ordered soft system relax due to the Jahn-Teller distortion of the surrounding Te atoms. Such a relaxation shifts the acceptor level above Fermi energy, resulting in a formation of neutral Te-enriched region. Perspectively, the shift up could convert the Te level to become donor.

In the third interval ($T > 1160°C$) the σ and R_H increase moderately in comparison with the lower T resulting to the slope 0.8 eV. We interpret such a behaviour as a hybridization of the conduction band with the Cd or Te impurity band. The liquid comes to be a semimetallic degenerate system. The defects are not fully ionized and the system cannot be described successfully within a simple semiconductor model. We cannot distinguish from our measurements if the Cd or the Te impurity band is responsible for such effect. In view of the good agreement of σ with the data of [49,54] where their experimental setup resulted probably into increased contents of Te in the liquid, we prefer hybridization with the Te impurity band.

Evaluation of all data is complicated by the fact, that Cd or Te pressure in the measuring cell are not well defined in the present setup. Improvement in precision and understanding of results of GM measurements near the melting point of CdTe can be reached, if a new setup enabling measurements in more defined conditions is constructed.

VI. CONCLUSION

This final report comprises a complex view of defect structure of CdTe based on high temperature GM measurements below and above the melting point, when a model based on Cd interstitials and Cd vacancies as dominating native defects is applied. The possible role of Te antisite within the model is discussed.

REFERENCES

[1] M. A. Berding, Appl. Phys. Lett. **74**, 553 (1999).

[2] V. Godlevsky, M. Jain, J. Derby, and J. R. Chelikowsky, Phys. Rev. **B60**, 8640 (1999).

[3] B. Segall, M. R. Lorenz, and R. E. Halsted Phys.Rev.**129**, 2471 (1963).

[4] D. J. Howarth and E. H. Sondheimer, Proc. Roy. Soc. **219A**, 53 (1953).

[5] O. Kane, in *Semiconductors and Semimetals* Vol. 1, edited by R. K. Willardson, A. C. Beer (Academic Press, New York, 1966) p.75.

[6] F. T. J. Smith, Met. Trans. **1**, 617 (1970).

[7] S. S. Chern, H. R. Vydyanath, and F. A. Kröger, Journal of Solid St. Chem. **14**, 33 (1975).

[8] D. L. Rode, Phys. Rev **B2**, 4036 (1970).

[9] D. L. Rode, in *Semiconductors and Semimetals* Vol. 10, edited by R. K. Willardson, A. C. Beer (Academic Press, New York, 1975) p.1.

[10] A. Wall, Y. Gao, A. Raisanen, A. Franciosi, and J.R.Chelikowski, Phys. Rev. **B43**, 4988 (1991).

[11] O. Madelung (Ed.), *Semiconductors - Basic Data*, 2nd rev. Ed. (Springer, Berlin, 1996) p.267.

[12] P. N. Butcher and W. Fawcett, Proc. Phys. Soc. (London) **86**, 1205 (1965).

[13] C. Jacoboni, L. Reggiani, Phys. Lett. **33A**, 333 (1970).

[14] B. R. Nag, *Electron Transport in Compound Semiconductors* (Springer, Berlin, 1980) p.372.

[15] D. Nobel, Philips Res. Rep. **14**, 361,430 (1959).

[16] Sundha Gopalan, P. Lautenschlager, and M. Cardona, Phys. Rev. **B35**, 5577 (1987).

[17] R.C.Whelan and D.Shaw, Phys.Stat.Sol.29, 145 (1968)

[18] O.A.Matveev, Yu.V.Rud and V.Sanin, Sov.Phys.Semicond.3, 779 (1969)

[19] K.R.Zanio, Appl.Phys.Lett.15, 260 (1969)

[20] H. R. Vydyanath, J. Ellsworth, J. Kennedy, B. Dean and C. J. Johnson, J. Vac. Sci. Technol. B10, 1476 (1992)

[21] P. Fochuk, O. Korovyanko and O. Panchuk, J. Cryst. Growth 197, 603 (1999).

[22] M. Wienecke, H. Berger and M. Schenk, Mater. Sci. Eng. B16, 219 (1992)

[23] M. Wienecke, M.Schenk and H.Berger, Semicond.Sci.Technol.8, 299 (1993)

[24] O. Panchouk, P. Fochouk and P. Feichouk, J. Cryst. Growth 161, 144 (1996) Journal of Solid St. Chem. **14**, 33 (1975).

[25] R. Grill, L. Turjanska, P. Höschl, J. Franc, and E. Belas, to be published.

[26] M. A. Berding, M. van Schilfgaarde, and A. Sher, Phys. Rev. B50 1519 (1994).

[27] G. L. Hansen, J. L. Schmit and T. N. Casselman, J. Appl. Phys. 53, 7099 (1982)

[28] C.H.Su, P.K.Liao and R.F.Brebrick, J.Electron.Mater.12, 771 (1983)

[29] J. Franc, R. Grill, L. Turjanska, P. Höschl, E. Belas, and P. Moravec, J.App.Phys., to be published

[30] K. K. Kavazawa, F.C.Brown, Phys.Rev.135, A1757 (1964)

[31] O. A. Matveev, A. I. Terentev, Fiz. tekh. polup. 32, 159 (1998)

[32] D.Kranzer, Phys.Stat.Sol(a) 26, 11 (1974)

[33] D. Look in Semiconductors and Semimetals 38, p.91, Academic Press, 1993

[34] P. Emanuelsson, P.Omling, B.K.Meyer, M.Wienecke and M.Schenk, Phys. Rev. B47 (1993) 15578.

[35] M.R.Lorenz, B.Segall, Phys.Lett.7, 18 (1963)

[36] J. V. Rud, K. V. Sanin, Fiz. tekh. polup. 5, 284 (1971)

[37] J. H. Greenberg, J. Crystal Growth 197, 406 (1999)

[38] R. Fang and R. F. Brebrick, J. Phys. Chem. Sol. 57, 443 (1996)

[39] M. A. Berding, Nucl. Instr. and Methods A, to be published in (2000)

[40] B.K.Meyer, P.Omling, E.Wiegel and G.Mueller-Vogt, Phys.Rev.B46, 15135 (1992)

[41] B.K.Meyer, W.Stadler, J.Crystal Growth 161, 119 (1996)

[42] M. R. Lorenz, J.Phys.Chem.Sol. 23, 939 (1962).

[43] R. F. Brebrick, J.Electrochem.Soc. 118, 2014 (1971).

[44] J. H. Greenberg, V. N. Guskov, V. B. Lazarev and O. V. Shebershneva, J.Solid State Chem. 102, 382 (1993).

[45] Rei Fang and R. F. Brebrick, J.Phys.Chem.Sol. 57, 443 (1993).

[46] T. C. Yu and R. F. Brebrick, J.Phase Equilibria 13, 476 (1992).

[47] R. F. Brebrick, Ching-Hua Su, and Pok-Kai Liao, In Semiconductors and Semimetals (Ed. by R. K. Willardson and A. C. Beer), Vol. 19, p. 171. Academic Press, New York (1983).

[48] J. P. Gaspard, C. Bergman, C. Bichara, R. Bellissent, P. Chieux and J. Goffart, J. Non-Crystalline Solids 97-98, 1283 (1987).

[49] V. Glazov, S. Chizhevskaya, and N. Glagoleva, Liquid Semiconductors (Plenum Press, New York, 1969).

[50] L. Shcherbak, J.Crystal Growth 197, 397 (1999).

[51] H.N.G. Wadley, B.W.Choi, J.Crystal Growth 172, 323 (1997).

[52] J.Gaspard, J.Y.Raty, R.Ceolion and R.Bellissent, J.Noncrystalline Sol.205-207, 75 (1996)

[53] J.V.Rud, K.V.Sanin, Fiz.tekh.polup. 5, 284 (1971)

[54] L. Shcherbak, J.Crystal Growth 197, 397 (1999).

[55] P. Höschl,E. Belas, L. Turjanska, R. Grill, J. Franc, R.Fesh and P. Moravec, to be published, J.Cryst.Growth

[56] V.V.Godlevsky, J.J.Derby and J.R.Chelikowski, Phys.Rev.Lett.81, 4959 (1998)

[57] J. Franc, R. Grill, L. Turjanska, P. Höschl, E. Belas, and P. Moravec, to be published

TABLES

TABLE I. The ionization energy and degeneracy of Cd_I and V_{Cd}. All defects are divalent. The two energies for the Cd_I correspond to the two tetrahedral interstitial sites (*ab initio*). The V_{Cd} energies are referenced in the Table, other data are acording to [1,39]

Defect	E^1(meV)	g_1	E^2(meV)	g_2
Cd_I	0; 210	2	170; 360	1
V_{Cd}	50 [35]	2	470 [34]	1/3
Te_{Cd}	0	2	390	1/3
V_{Te}	1400 [40]	2	1800 [41]	1

TABLE II. The *ab initio* calculated energy and entropy terms and the respective values which were used in the fit of experimental data. The underlined parameters were optimized. The two energies for the *ab initio* Cd_I correspond to the two tetrahedral interstitial sites.

	ab initio		fit	
Defect	$E+U^{vib}$(eV)	$S(k_b)$	$E+U^{vib}$(eV)	$S(k_b)$
Cd_I	0.96; 1.29	8.8	0.96; 1.29	<u>11.1</u>
V_{Cd}	3.24	-8.2	<u>3.35</u>	<u>-5.6</u>
Te_{Cd}	4.72	-17	<u>$\geq$6</u>	-17